Catalysis Today 138 (2008) 43–49

Contents lists available at ScienceDirect

Catalysis Today

journal homepage: www.elsevier.com/locate/cattod

H_2-induced promotion of CO oxidation over unsupported gold

Elodie Quinet [a], Laurent Piccolo [a,*], Helen Daly [b], Frédéric C. Meunier [b,1], Franck Morfin [a], Ana Valcarcel [a], Fabrice Diehl [c], Priscilla Avenier [c], Valérie Caps [a,*], Jean-Luc Rousset [a]

[a] Institut de recherches sur la catalyse et l'environnement de Lyon (IRCELYON, UMR 5256 CNRS/University of Lyon), 2 Avenue Albert Einstein, 69626 Villeurbanne Cedex, France
[b] CenTACat, Queen's University Belfast, David Keir Building, Stranmillis Road, Belfast, Northern Ireland BT9 5AG, United Kingdom
[c] IFP Lyon, BP n̊3, 69390 Vernaison, France

ARTICLE INFO

Article history:
Available online 16 June 2008

Keywords:
Unsupported gold
CO oxidation
PrOx
Promotion by hydrogen

ABSTRACT

The kinetics and mechanism of the preferential oxidation of carbon monoxide in the presence of hydrogen (PrOx) over an unsupported gold powder (mean particle size ~20 nm and free of silver) have been investigated using flow fixed bed catalytic testing and diffuse reflectance infrared Fourier transform spectroscopy coupled to mass spectrometry (*operando* DRIFTS or DRIFTS-MS). It is shown that the presence of H_2 has a favourable effect on the oxidation of CO, either by strongly accelerating the reaction or by preventing the catalyst deactivation, depending on the conditions used. Variation of the hydrogen partial pressure has allowed us to determine partial reaction orders for both CO oxidation and H_2 oxidation under PrOx conditions. An infrared band at ~2113 cm^{-1}, corresponding to on-top CO adsorption on metallic gold, has been observed below 150 °C. In addition, adsorbed hydroxyl groups gradually develop simultaneously to gas-phase water in the course of the reaction at increasing temperatures. The promotional effect of hydrogen is ascribed to highly oxidative H_xO_y intermediates formed from the interaction between H_2 and O_2 on the gold surface.

© 2008 Elsevier B.V. All rights reserved.

1. Introduction

Gold is known as the noblest of all metals [1]. However, since the work of Haruta's group in the late 1980s, supported gold nanoparticles are well-known for their ability to catalyze a variety of reactions under mild conditions. In particular, the oxidation of carbon monoxide has been widely studied due to its interest in e.g. air decontamination and hydrogen fuel purification [2–5]. The support of the nanoparticles has been found critical to activate molecular oxygen for CO oxidation [6,7]. Unlike Al_2O_3, reducible supports like TiO_2 exhibit high synergy with gold.

Conversely, pure bulk gold is inert for the CO–O_2 reaction, unless O_2 is pre-dissociated [8–11]. In their study of a gold powder [12], Iizuka et al. have found a strong correlation between the (non-zero) catalytic activity and the surface concentration of Ag impurities. Recently, unsupported nanoporous gold was reported to exhibit unexpected high activity for CO oxidation [13–15]. However these results could most likely be explained by the presence of Ag impurities, due to the preparation method (Ag–Au alloys treated by acids), as recently discussed by Haruta [16]. Besides, a striking result was obtained by Sanchez-Castillo et al., who could oxidize CO with water using gold-nanotube membranes [17]. Water and hydrogen have been shown to generally promote the activity for CO oxidation of supported gold catalysts for which oxygen activation is rate-limiting [18–21]. These molecules have a smaller impact on the CO oxidation rates observed over gold nanoparticles associated with reducible oxides [22,23].

Here we demonstrate that an unsupported gold powder, initially weakly active for CO oxidation, can be activated or regenerated by the presence of H_2 in the reaction feed. The onset of catalytic activity is correlated to the appearance of an infrared (IR) band related to CO adsorption on metallic gold.

2. Experimental

2.1. Material characterization

A gold nanopowder (99.9% Au, 9 m^2 g^{-1}) was purchased from Nanostructured & Amorphous Materials Inc. It was analyzed by inductively coupled plasma atom emission spectroscopy (ICP-AES)

* Corresponding authors. Tel.: +33 472 445 331; fax: +33 472 445 399.
E-mail addresses: laurent.piccolo@ircelyon.univ-lyon1.fr (L. Piccolo), valerie.caps@ircelyon.univ-lyon1.fr (V. Caps).
[1] Present address: Laboratoire Catalyse et Spectrochimie, CNRS and University of Caen, ENSICAEN, 6 Boulevard du Maréchal Juin, 14050 Caen Cedex, France.

0920-5861/$ – see front matter © 2008 Elsevier B.V. All rights reserved.
doi:10.1016/j.cattod.2008.04.042

at the CNRS Center for Chemical Analysis (Vernaison, France). The main impurities present were Fe (0.52 wt.%), Ni (0.11 wt.%) and Cu (0.02 wt.%). Traces of Pb (25 wt. ppm), Al (24 wt. ppm) and Ag (21 wt. ppm) were also detected. As mentioned below, only Cu was detected at the powder surface. X-ray diffraction (XRD, Bruker D5005 diffractometer, Cu $K_{\alpha 1+\alpha 2}$ radiations (λ = 1.54184 Å), 2θ range of 3–80° at a rate of 0.02 s^{-1}) showed that the powder is composed of crystallites with a mean size of 20 nm, exhibiting mainly (1 1 1) facets. Transmission electron microscopy (TEM, JEOL 2010 microscope operated at 200 kV) revealed that the grain size is quite heterogeneous with some small particles (~20 nm) and also large, polycrystalline aggregates of more than 500 nm. Further characterization by thermogravimetric/differential thermal analysis coupled mass spectrometry (TG–DTA–MS, Setaram Instrumentation SETSYS Evolution – 1200 apparatus) under air and under hydrogen (flows of 50 cm^3 min^{-1}; ramps from 20 to 350 °C at 5 min^{-1}) allowed to determine a suitable thermal treatment for cleaning/activating the gold powder. This treatment consisted in calcination at 350 °C for 2 h followed by in-situ reduction under 5%H_2/He (50 cm^3 min^{-1}) at 350 °C for 2 h. This caused an increase in the average crystallite size to 40 nm (XRD) due to sintering of the unsupported gold particles. However, it also allowed to remove organic residues (as shown by CO_2 and H_2O evolutions at 250 and 280 °C) which also contained nitrogen, as shown by X-ray photoelectron spectroscopy (XPS) before and after the treatment. XPS surface analysis was carried out under ultra-high vacuum ($P < 10^{-9}$ mbar) with a Kratos Axis Ultra DLD spectrometer using monochromated Al Kα radiation (1486.6 eV, 150 W), a pass energy of 40 eV and a hybrid lens mode. The binding energy scale was corrected for surface charging by taking the C 1s peak of contaminant carbon as a reference at 284.6 eV. The binding energy of the Au $4f_{7/2}$ core level in the pretreated powder was found at 84.2 eV, which is that of metallic gold (Au^0). The only other element detected by XPS was copper, with a surface concentration of 1.5 at.%. The binding energy of the Cu $2p_{3/2}$ peak found at 932.3 eV is not consistent with that of CuO but could be attributed to either Cu or Cu_2O [24]. As Cu_2O easily oxidizes to CuO, we tested a CuO powder under the same conditions as those used for evaluating the gold nanopowder (Section 2.2). We found that the contribution of the copper impurity to the overall activity of the gold powder does not exceed 3%. As the other impurities measured by ICP, and especially silver, are absent from XPS spectra and thus from the gold surface, they should therefore not contribute to the observed catalytic behaviour. Thus, despite its broad particle size distribution, this gold powder remains the purest used to study CO oxidation over naked gold.

2.2. Catalytic measurements

The kinetics of the preferential oxidation of CO in hydrogen (PrOx) were measured in a continuous flow fixed bed reactor at atmospheric pressure and variable temperature [21], with various amounts of hydrogen in the reactant gas mixture. 200 mg of the calcined (air/350 °C/2 h) gold powder (1 mmol Au) were introduced in the quartz tube reactor located in a ceramic furnace. The Au powder was then pretreated in-situ in 5%H_2/He (50 cm^3 min^{-1}) at 350 °C for 2 h. The reactant gases were mixed using mass flow controllers (Brooks Instrument) and sent through the reactor at a total flow rate of 50 mL min^{-1} corresponding to a gas hourly space velocity (GHSV) of ~5 h^{-1}. The gas mixtures consisted in CO(2%) + O_2(2%) + H_2(*x*%) (*x* = 0–48), balanced in helium. The reaction was temperature-programmed between ambient and 230 °C with a heating rate of 1 min^{-1}. Two thermocouples located inside the catalytic bed allowed to control the furnace heating power and acquire the reaction temperature that is used to plot the light-off curves. Two reaction cycles, each consisting of a heating and a cooling period, were recorded, which allowed to observe that the powder was further activated under the reaction conditions used (CO + O_2 + H_2 mixture). Thus, the data corresponding to the second cooling step are plotted here and used for discussion. The outlet gases were analyzed with an online Varian-Micro GC (CP2003) equipped with a TCD detector. Two columns were used in parallel: a Molsieve 5A column (Ar as carrier gas) to quantify H_2, O_2 and CO and a poraPLOT Q column (He as carrier gas) to quantify CO_2.

Mass-specific CO or H_2 oxidation rates (mol g_{Au}^{-1} s^{-1}) were determined from the concentration of each component at the in- and outlets of the reactor using the following formula:

$$r_{CO} = \frac{y_{CO,in} X_{CO} V_{gas}}{m_{Au}} \quad \text{or} \quad r_{H_2} = \frac{y_{H_2,in} X_{H_2} V_{gas}}{m_{Au}}$$

where: m_{Au} = mass of Au in the catalytic bed in g, V_{gas} = total molar flow rate in mol s^{-1}, X_{CO} (X_{H_2}) = conversion of CO (conversion of H_2), Note: X_{CO} is calculated on the basis of CO_2 formation $y_{CO,in}$ ($y_{H_2,in}$) = molar fraction of CO (H_2) in the inlet gas mixture

Selectivity to CO_2 at a given temperature in the PrOx reaction is defined as $r_{CO}/(r_{CO} + r_{H_2})$.

2.3. DRIFTS-MS experiments

The apparatus has been described previously [25]. Briefly, the experimental setup consisted of an in-situ high-temperature diffuse reflectance infrared cell (from Spectra-Tech) fitted with ZnSe windows. The DRIFTS cell was located in a Vertex 70 FTIR spectrometer from Bruker, operating at a resolution of 4 cm^{-1}. The reactor crucible was modified to ensure plug-flow conditions throughout the catalyst bed: the original porous bed supporting the sample was replaced by an inert metallic mesh and Teflon tape was used to seal the gap between the ceramic crucible and the metallic base plate. The reaction flow was going down the reactor bed. Therefore, the upper layer of the catalyst (which is probed by the DRIFTS technique) was the front of the bed. The cell was connected to the feed gas cylinders through low-volume stainless-steel lines. A cold trap containing solid CO_2 and acetone was used to avoid possible contamination of the catalyst by the feed gases. The gas flows were controlled by Aera mass flow controllers. The cell outlet was connected to a Hiden Analytical HPR20 quadrupole mass spectrometer via a warm capillary. The amount of catalyst used in the DRIFTS reactor was 75 ± 5 mg. The DRIFTS data are reported as log 1/*R* (pseudo-absorbance), with $R = I/I_o$, where *R* is the sample reflectance, I_o is the intensity measured on the sample after exposure to the argon feed and *I* is the intensity measured under reaction conditions.

The Au powder was pretreated at 350 °C in a flow of O_2 (20% in Ar) for 2 h, then H_2(20% in Ar) for 2 h. Then the sample was cooled down to 50 °C by steps of 50 °C in order to record reference spectra under pure Ar flow at each temperature of interest. At 50 °C, CO(2%) was introduced into the feed, then CO(2%) + O_2(2%), then CO(2%) + O_2(2%) + H_2(10%). The total flow rate was 100 mL min^{-1} in all the cases. At each step, several IR spectra were recorded. Then O_2 and H_2 supplies were shut off and the temperature was raised to 100, 150, 200 and 350 °C, following a similar procedure at each temperature. Only for 200 °C several H_2 molar fractions were tested (2, 5, 10 and 20%). Then the powder temperature was set back to 100 °C in order to assess the influence of the high-temperature stage on the reaction kinetics and the IR features.

The masse/charge ratios 12, 14, 18, 28, 32, 36 and 44, corresponding to carbon, nitrogen, water, CO, O_2, Ar and CO_2, respectively, were continuously recorded by MS.

3. Results

3.1. Kinetic study

The effects of hydrogen on the oxidation rate of CO have been studied by varying the H_2 concentration in the PrOx reaction. Oxidation rates of CO and H_2, selectivity to CO_2 and O_2 conversion as a function of temperature and H_2 molar fraction are reported in Fig. 1a–d, respectively. Some key kinetic data (apparent activation energies, reaction rates and selectivity) are summarized in Table 1.

In the absence of H_2, the CO oxidation rate observed over the gold nanopowder is very low (Fig. 1a). CO conversion reaches only a few percent at 200 °C. This is about 3 orders of magnitude lower than that observed on an Au/Al_2O_3 catalyst [21]. Even by taking into account that gold is about 10 times less dispersed than in the supported catalysts (for example Au/TiO_2 or Au/Fe_2O_3 reference catalysts [26]), the activity of pure gold remains significantly lower than that of oxide-supported gold nanoparticles.

The introduction of hydrogen in the reactant feed results in an increase of the CO oxidation rate, as we observed over alumina-supported gold catalysts [23]. For these materials, hydrogen has been reported to activate O_2 apparently just like reducible oxides [27]. Similarly, in the present case, the PrOx reaction proceeds with 100% selectivity towards CO_2 at low temperature (Fig. 1c). This shows that, for both unsupported and supported gold catalysts, the O_2 activation step, which is rate-determining in $CO–O_2$ mixtures, is facilitated in PrOx mixtures.

As the temperature increases ($T > 100$ °C), hydrogen starts to be oxidized to water (Fig. 1b), thus competing with CO for reaction with oxygen. This results in a decrease in the selectivity to CO_2 as the temperature increases. For high concentrations of hydrogen, CO conversion starts to level off (Fig. 1a) from the temperature at which O_2 begins to lack from the feed (Fig. 1d). This is due to preferential consumption of oxygen for H_2 oxidation, as deduced from the higher apparent activation energy found for H_2 oxidation vs. CO oxidation, whatever the concentration of hydrogen in the feed (see Arrhenius diagrams plotted in Fig. 2). Apparent activation

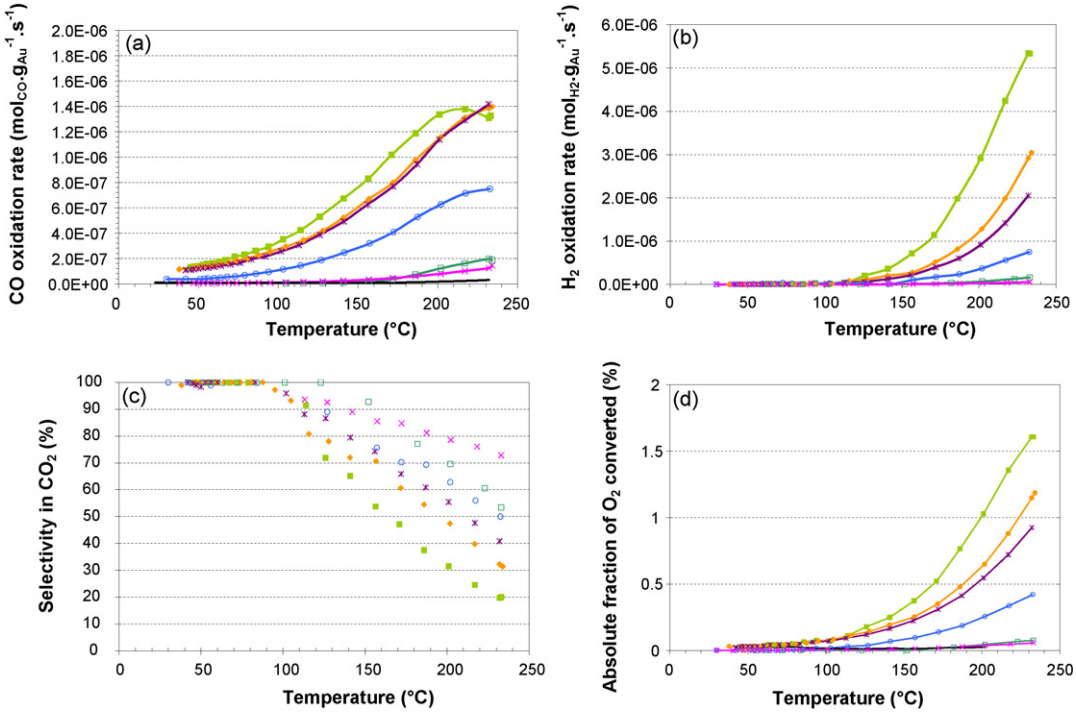

Fig. 1. CO oxidation rate (a), H_2 oxidation rate (b), selectivity to CO_2 (c) and O_2 conversion (d) vs. temperature in the PrOx reaction over the gold powder, using various molar fractions of H_2 in the reactant feed: 0%, (×) 0.25%, (□) 1%, (○) 5%, (*) 10%, (◆) 20%, (■) 48%.

Table 1
Catalytic properties of the unsupported gold nanopowder in the PrOx reaction using various concentrations of hydrogen

$y_{H_2,in}$%[a]	Ea (kJ mol^{-1})[b]		T (°C)[c] $r_{COprox} \cap r_{H_2PrOx}$	Reaction rates[d] (μmol g_{Au}^{-1} s^{-1})		Sel[e] (150 °C)%
	COPrOx	H_2PrOx		COPrOx	H_2PrOx	
0	29	–	–	0.005	–	–
0.25	29	52	>250	0.010	0.03	83
1	32	56	235	0.004	0.07	76
5	25	54	233	0.107	0.36	85
10	20	55	212	0.249	0.87	77
20	20	48	197	0.273	1.21	72
48	19	52	165	0.329	2.83	58

[a] Mole fraction of hydrogen in the PrOx reaction mixture.
[b] Apparent activation energies (standard deviation <1 kJ mol^{-1}) for the oxidations of CO (COPrOx) and H_2 (H_2PrOx) in the PrOx reaction, as calculated from Fig. 2.
[c] Temperature at which the rate of H_2 oxidation (r_{H_2PrOx}) becomes higher than that of CO oxidation (r_{COPrOx}) in the PrOx reaction.
[d] Reaction rates given at 100 °C for COPrOx and at 200 °C for H_2PrOx.
[e] Selectivity to CO_2 in the PrOx reaction at 150 °C.

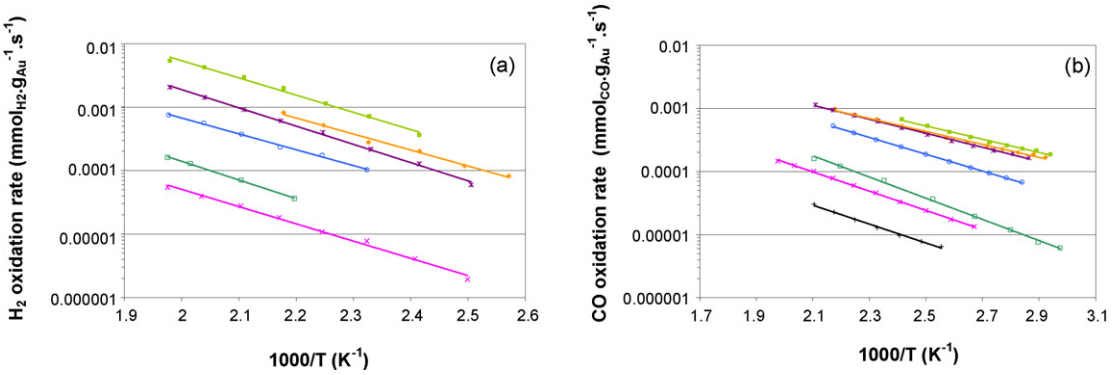

Fig. 2. Determination of activation energies (Table 1) for the Au-catalyzed oxidations of CO (a) and H_2 (b) in PrOx mixtures, using various concentrations of H_2 in the reactant feed: (×) 0.25%, (□) 1%, (○) 5%, (*) 10%, (◆) 20%, (■) 48%. Only the points corresponding to a conversion of the minor reactant below 20% are plotted.

energies for the oxidation of H_2 are indeed about 48–56 kJ mol^{-1} while those for the oxidation of CO vary between 19 kJ mol^{-1} and 32 kJ mol^{-1} (Table 1). The latter tends to slightly decrease with increasing concentration of hydrogen in the feed. These apparent activation energies observed over the pure gold nanopowder are similar to those obtained over highly dispersed alumina-supported gold nanoparticles [21].

The partial reaction orders with respect to H_2, on the other hand, are higher than those obtained on the alumina-supported catalyst, which indicates that the promotional effect of hydrogen (i.e., the CO oxidation rate increase with increasing hydrogen molar fraction in the feed) is more marked on this unsupported gold catalyst. We find $\alpha_{H_2}^{COPrOx} = 1.12 \pm 0.01$ and $\alpha_{H_2}^{H_2PrOx} = 0.88 \pm 0.03$ for the oxidations of CO (100 °C) and H_2 (200 °C, 10^3–10^4 Pa range), respectively, as determined from Fig. 3, instead of 0.24 and 0.58 for Au/Al_2O_3 [21]. Note that increasing the H_2 pressure above 10^4 Pa does not lead to a further increase in the CO oxidation rate, indicating that the promotional effect of H_2 on the gold-catalyzed CO oxidation reaches saturation for the higher concentrations of hydrogen in the feed. A more significant variation of activity at low hydrogen fractions was also observed on Au/Al_2O_3 [21].

3.2. DRIFTS-MS study

Fig. 4 shows the variations of CO_2 and H_2O MS signals with time all along the DRIFTS-MS experiment, following the initial oxidative and reductive treatments (see Section 2.1). Note that the activity of the powder for CO oxidation was negligible before this treatment.

At each temperature, the introduction of O_2(2%) in the CO(2%) + Ar feed induces a sudden increase of the CO_2 signal, which then decreases, but the deactivation rate also decreases with time. Thus the oxidative–reductive treatment allowed the onset of CO oxidation on the gold powder. Going from 100 to 300 °C, the CO_2 formation rate increases and so does the initial deactivation rate. The maximum measured conversion of CO to CO_2 over the whole experiment is ~20% at 300 °C. It is possible that the non-zero CO oxidation rate measured in these experiments (contrary to kinetic experiments, Section 3.1 in the absence of H_2 is due to traces of water present in the feed.

Below 200 °C, introduction of H_2(10%) increases the CO_2 signal to a stable value. This means that at low temperature, the presence of H_2 promotes CO oxidation, as also noted in Section 3.1, and stops deactivation. At 200 °C, the CO_2 signal first suddenly decreases upon H_2 introduction, then it increases, but to a lower extent. However, deactivation no longer occurs. At this temperature, the overall decrease in CO_2 production may be ascribed to competitive adsorption of O_2 and H_2, since oxygen chemisorption becomes significant from ~200 °C and above, as will be discussed

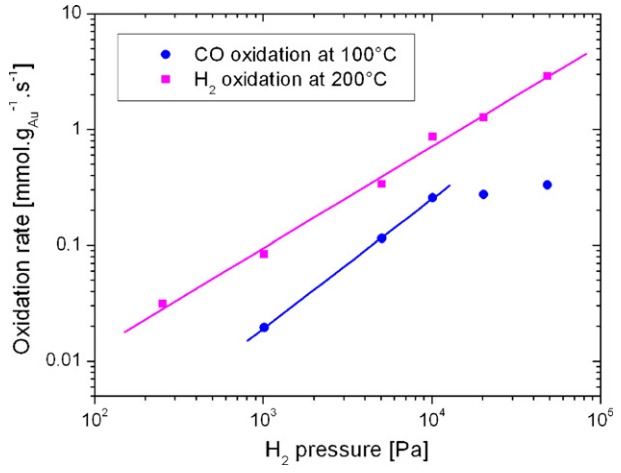

Fig. 3. Logarithmic plot of reaction rates vs. hydrogen partial pressure allowing the determination of the hydrogen partial reaction orders for the oxidation of CO (●) and the oxidation of H_2 (▲) in the PrOx reaction over unsupported gold at 100 and 200 °C, respectively.

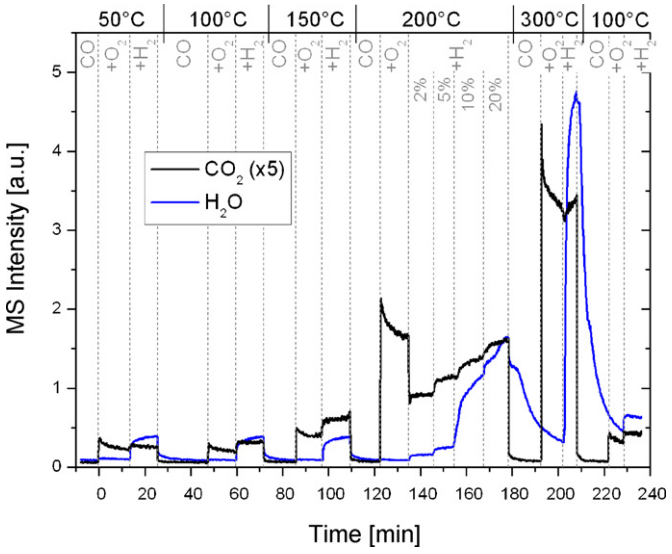

Fig. 4. Mass spectrometry signal as a function of time for mass/charge ratios 18 (H_2O) and 44 (CO_2). The flowing gas composition is indicated at the top. CO, O_2 and H_2 molar fractions were 2%, 2% and 10%, respectively, except when specified. The reactive mixture was balanced in Ar in all the cases. NB: the sensitivities of MS to CO_2 and H_2O are similar.

in Section 4 At 200 °C, increasing the H_2 molar fraction gradually restores the activity reached in the CO + O_2 feed. The gradual increase in CO_2 production with time in the CO + O_2 + H_2(20%) mixture indicates that the initial activity could be restored upon longer reaction run. Hence, at high temperature, the presence of H_2 reverses the deactivation tendency exhibited by the gold powder. The origin of this deactivation is unknown since no carbonate-like species, the formation of which is responsible for the deactivation of oxide-supported gold catalysts [5,34], are detected by DRIFTS on the gold powder (Fig. 6).

In all the cases, introduction of H_2(10%, except at 200 °C: 2–20%) in the CO + O_2 + Ar feed leads to an increase (fast, then slow) of the water signal, the amplitude of which is greater at the higher temperatures. At 200 °C, it is seen that water formation increases with H_2 content. The largest increase is observed when the molar fraction of H_2 is switched from 5 to 10%, whilst the extent of the promotional effect of H_2 on CO_2 formation does not depend on H_2 pressure. As also noted in Section 3.1 (Fig. 1c), the H_2 oxidation pathway is favoured over CO oxidation at high temperature, i.e., selectivity to CO_2 is lower, and it decreases as the H_2 pressure increases.

In addition, water disappears more slowly than CO_2 after H_2 and O_2 are switched off. While at low temperature (<200 °C), CO_2 and H_2O levels quickly drop to their initial value when the supply of O_2 and H_2 in the feed is stopped, the larger amount of water is evacuated quite slowly at higher temperatures (200 and 300 °C).

When the temperature is set back to 100 °C, CO_2 and H_2O formation rates are moderately higher than those were at this temperature before heating up to 300 °C under reactive mixture. Further activation of the catalyst under reaction conditions was also observed during our kinetic experiments, as noted in Section 2.2.

Fig. 5 shows the C–O stretching vibration region of DRIFTS spectra recorded at various steps of the experiment described above. The gas-phase CO contribution was subtracted from these spectra. A band centred at 2112–2114 cm^{-1} is present at 50 °C on the pretreated powder. It corresponds to linear adsorption of CO molecules on-top of metallic gold atoms [28–34]. This peak becomes less intense at 100 °C but remains present, whereas it was not observed before pretreatment. This correlates with the negligible activity of the gold particles before activation, which could be due to the poisoning of active sites by contaminants such as hydrates, carbonates or N-containing species, as shown by XPS and TG–DTA–MS studies (Section 2.1).

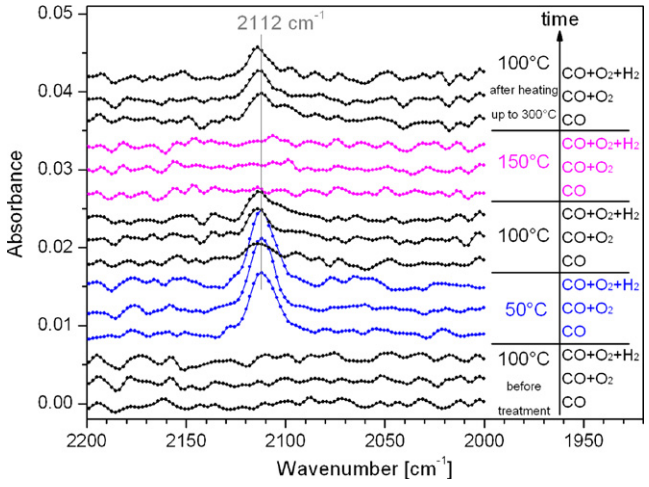

Fig. 5. Series of DRIFTS spectra (carbonyl region) recorded for the Au powder under the experimental conditions mentioned on the picture right-hand side (same as Fig. 4). The gas-phase CO contribution was subtracted from the spectra.

The carbonyl peak is no longer present at 150 °C and above, the CO coverage becoming lower as temperature increases. In other words, the residence time of the CO molecules on the gold surface decreases. There is no significant influence of the presence of O_2 and H_2 in the feed on the CO/Au peak intensity and position. This can be ascribed to the low coverage of CO on gold, even at low temperature, which prevents competitive adsorption and coupling effects. After heating the sample up to 300 °C, the intensity measured at 100 °C is unchanged.

The only other features exhibited by DRIFTS spectra relate to gas-phase CO_2 and H_2O, and to bonded hydroxyl groups in the presence of O_2 and H_2. Indeed, as shown by Fig. 6, a broad band at 3100–3500 cm^{-1}, corresponding to the O–H stretching vibration, grows as temperature increases from 50 to 300 °C, in parallel to water accumulation in the system. The OH band slightly decreases when returning to 100 °C. No peak is observed around 1623 cm^{-1}, which implies that there is no adsorbed H_2O on the gold surface [34]. The OH groups might be, lead to, or come from, highly oxidative adsorbates [35–39], which could be at the origin of the promoting effect of H_2, as discussed below.

4. Discussion

The production of CO_2 observed over the gold nanopowder, as described in both the cases of the catalytic reactor and the DRIFT-MS experiments, shows that gold can catalyze CO oxidation in the absence of any oxide support. The turnovers are however two orders of magnitude lower than those obtained over an alumina-supported catalyst [21] at isodispersion. This means that carbon monoxide and/or oxygen activations are less efficient on the unsupported gold particles. While CO readily chemisorbs on all gold surfaces [40] and nanoparticles [41] as well as on our powder (as shown by the DRIFTS experiments), the affinity of gold for oxygen is very low [42]. Oxygen adsorption has been shown (by experiments and calculations) to strongly depend on the Au cluster size [43,44]. It preferentially occurs on highly defective surfaces and on small gold nanoparticles, which bear a high concentration of low-coordination sites (kinks, edges. . .) [45]. The large size of the gold particles in the nanopowder (~20 nm) is thus likely to limit oxygen chemisorption.

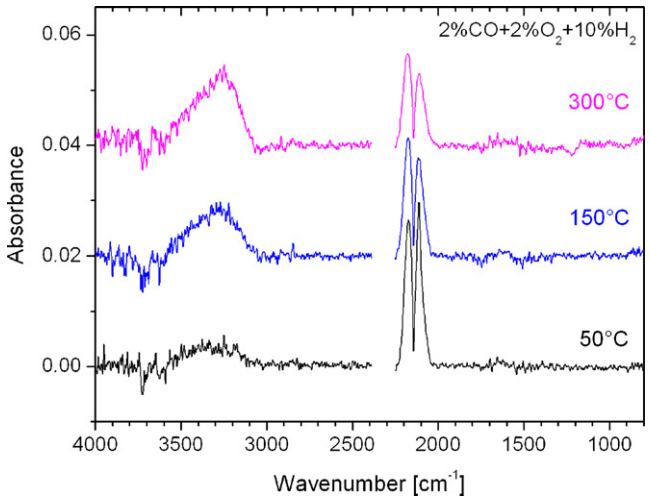

Fig. 6. Series of DRIFTS spectra for the Au powder. The atmospheric water component was subtracted from the spectra, and the atmospheric CO_2 contribution at 2390–2250 cm^{-1} was deleted for sake of clarity. The negative bands in the range 3750–3550 cm^{-1} are due to atmospheric CO_2. The two bands in the range 2250–2000 cm^{-1} correspond to (both gas-phase and adsorbed) carbon monoxide.

Another difference between supported and unsupported gold particles is the oxidation state of gold. The Au^0 unsupported particles (XPS, DRIFTS) are expected to be less favourable to oxygen chemisorption [46,47] than the electron-rich gold particles supported on alumina [21]. The O–O bond has been shown to be less activated on neutral gold clusters than on free Au cluster anions. However, our catalytic and DRIFTS data give experimental evidence for the existence of the predicted [48,49] support-free pathway for CO oxidation.

In the presence of hydrogen, the gold nanopowder remains much less active than the alumina-supported gold particles. Nevertheless, hydrogen has a stronger influence on the unsupported gold particles than on the supported catalyst, as shown by the higher H_2 partial reaction orders found for both CO and H_2 oxidations under PrOx conditions. Transient DRIFTS-MS studies also show that hydrogen immediately enhances CO_2 production (Fig. 4) at least up to 150 °C.

From 200 °C, the introduction of hydrogen in a $CO + O_2$ feed initially decreases the amount of CO_2 produced, which could result from a competitive adsorption between O_2 and H_2. Indeed, since the amount of powder used in DRIFTS experiments is ~3 times lower than that used in the kinetic measurements, the reactant coverage at the gold surface is higher in the former case. Moreover, chemisorption of both O_2 [50] and H_2 [51] on Al_2O_3-supported gold catalysts is an activated process (i.e., the amount of adsorbed molecules increases with increasing temperature), which starts to be significant from 200 °C [52]. Increasing the hydrogen concentration at 200 °C then leads to a marked increase in the amounts of both CO_2 and H_2O produced (Figs. 1 and 4).

These results show that hydrogen directly enhances the activation of CO and/or O_2 on the gold nanopowder. The apparent energy barrier for CO oxidation is indeed lowered in the presence of higher molar fractions of hydrogen in the feed (Table 1). As hydrogen does not seem to have any influence on the oxidation state of gold (at least at low temperature, where the carbonyl band is clearly visible in Fig. 5) or on CO coverage, it is possible that, by reacting with oxygen, it generates intermediates that are more reactive than O_2 towards CO. In fact, theoretical calculations have shown that adsorbed hydrogen increases oxygen adsorption energy, leading to the formation of highly reactive hydroperoxo species [38]. Similarly, OOH and H_2O_2 species have been identified as intermediates during the reaction of H_2 and O_2 on supported gold articles [35,36]. Highly oxidative ad-species may also be in equilibrium with gas-phase water in the form of OH groups [37], which are indeed observed by DRIFTS (Fig. 6). In the latter case, the promotional effect of H_2 would be similar to that of H_2O [17,22,39], although no water is adsorbed at the surface under our conditions. In any case, low fractions of H_2 in the feed are enough to provide a significant "reservoir" of these promotional species on the gold surface. Increasing the hydrogen concentration only slightly changes its capacity (Figs. 1a and 3).

5. Conclusion

We have studied the effect of molecular hydrogen on CO oxidation over an unsupported silver-free gold powder, using conventional kinetic experiments and transient *operando* infrared analyses. Temperature and H_2 molar fraction in the feed have been varied in the ranges 25–300 °C and 0.25–48% (for 2%CO and 2%O_2), respectively. This study shows that the support-free pathway for the oxidation of CO exists and is enhanced by the presence of hydrogen. However, even with hydrogen, our unsupported particles are found to be less efficient than the oxide-supported ones to activate oxygen, probably because of a low concentration of low-coordination active sites present at the surface of large gold particles.

Acknowledgments

G. Bergeret, N. Cristin, P. Delichère, M.T. Gimenez, B. Jouguet, P. Mascunan and L. Massin are thanked for technical support in material characterization. LP and AV are grateful to Robbie Burch's group for receiving them at CenTACat laboratory through the EU funded Transnational Access Program.

References

[1] B. Hammer, J.K. Norskov, Nature 376 (1995) 238–239.
[2] G.C. Bond, D.T. Thompson, Gold Bull. 33 (2000) 41–51.
[3] M. Haruta, Gold Bull. 37 (2004) 27–36.
[4] M.S. Chen, D.W. Goodman, Science 306 (2004) 252–255.
[5] M. Azar, V. Caps, F. Morfin, J.L. Rousset, A. Piednoir, J.C. Bertolini, L. Piccolo, J. Catal. 239 (2006) 307–312.
[6] S. Arrii, F. Morfin, A.J. Renouprez, J.L. Rousset, J. Am. Chem. Soc. 126 (2004) 1199–1205.
[7] M. Comotti, W.C. Li, B. Spliethoff, F. Schüth, J. Am. Chem. Soc. 128 (2006) 917–924.
[8] D.A. Outka, R.J. Madix, Surf. Sci. 179 (1987) 351–360.
[9] J.M. Gottfried, K. Christmann, Surf. Sci. 566–568 (2004) 1112–1117.
[10] B.K. Min, A.R. Alemozafar, D. Pinnaduwage, X. Deng, C.M. Friend, J. Phys. Chem. B 110 (2006) 19833–19838.
[11] J. Kim, E. Samano, B.E. Koel, J. Phys. Chem. B 110 (2006) 17512–17517.
[12] Y. Iizuka, A. Kawamoto, K. Akita, M. Daté, S. Tsubota, M. Okumura, K. Haruta, Catal. Lett. 97 (2004) 203–208.
[13] V. Zielasek, B. Jürgens, C. Schulz, J. Biener, M.M. Biener, A.V. Hamza, M. Bäumer, Angew. Chem. Int. Ed. 45 (2006) 8241–8244.
[14] C. Xu, J. Su, X. Xu, P. Liu, H. Zhao, F. Tian, Y. Ding, J. Am. Chem. Soc. 129 (2007) 42–43.
[15] C. Xu, X. Xu, J. Su, Y. Ding, J. Catal. 252 (2007) 243–248.
[16] M. Haruta, ChemPhysChem 8 (2007) 1911–1913.
[17] M.A. Sanchez-Castillo, C. Couto, W.B. Kim, J.A. Dumesic, Angew. Chem. Int. Ed. 43 (2004) 1140–1142.
[18] R.J.H. Grisel, C.J. Weststrate, A. Goossens, M.W.J. Craje, A.M. van der Kraan, B.E. Nieuwenhuys, Catal. Today 72 (2002) 123–132.
[19] J.T. Calla, R.J. Davis, Ind. Eng. Chem. Res. 44 (2005) 5403–5410.
[20] D. Gavril, A. Georgaka, V. Loukopoulos, G. Karaiskakis, B.E. Nieuwenhuys, Gold Bull. 39 (2006) 192–199.
[21] E. Quinet, F. Morfin, F. Diehl, P. Avenier, V. Caps, J.-L. Rousset, Appl. Catal. B 80 (2008) 195–201.
[22] M. Daté, M. Okumura, S. Tsubota, M. Haruta, Angew. Chem. Int. Ed. 43 (2004) 2129–2132.
[23] C. Rossignol, S. Arrii, F. Morfin, L. Piccolo, V. Caps, J.-L. Rousset, J. Catal. 230 (2005) 476–483.
[24] S. Poulston, P.M. Parlett, P. Stone, M. Bowker, Surf. Interf. Anal. 24 (1996) 811–820.
[25] F.C. Meunier, D. Reid, A. Goguet, S. Shekhtman, C. Hardacre, R. Burch, W. Deng, M. Flytzani-Stephanopoulos, J. Catal. 247 (2007) 277–287.
[26] Gold reference catalysts, Gold Bull. 36 (2003) 24.
[27] V. Caps, S. Arrii, F. Morfin, G. Bergeret, J.-L. Rousset, Faraday Discuss. 138 (2008) 241–256.
[28] M.L. Kottke, R.G. Greenler, H.G. Tompkins, Surf. Sci. 32 (1972) 231–243.
[29] F. Boccuzzi, A. Chiorino, S. Tsubota, M. Haruta, J. Phys. Chem. 100 (1996) 3625–4363.
[30] Y. Jugnet, F.J.C.S. Aires, C. Deranlot, L. Piccolo, J.C. Bertolini, Surf. Sci. 521 (2002) L639–L644.
[31] T.V. Choudhary, C. Sivadinarayana, C.C. Chusuei, A.K. Datye, J.P. Fackler Jr., D.W. Goodman, J. Catal. 207 (2002) 247–255.
[32] D.C. Meier, V. Bukhtiyarov, D.W. Goodman, J. Phys. Chem. B 107 (2003) 12668–12671.
[33] S. Derrouiche, P. Gravejat, D. Bianchi, J. Am. Chem. Soc. 126 (2004) 3010–13015.
[34] B. Schumacher, Y. Denkwitz, V. Plzak, M. Kinne, R.J. Behm, J. Catal. 224 (2004) 449–462.
[35] C. Sivadinarayana, T.V. Choudhary, L.L. Daemen, J. Eckert, D.W. Goodman, J. Am. Chem. Soc. 124 (2004) 38–39.
[36] D.G. Barton, S.G. Podkolzin, J. Phys. Chem. B 109 (2005) 2262–2274.
[37] T.S. Kim, J. Gong, R.A. Ojifinni, J.M. White, C.B. Mullins, J. Am. Chem. Soc. 128 (2006) 6282–6283.
[38] L. Barrio, P. Liu, J.A. Rodriguez, J.M. Campos-Martin, J.L.G. Fierro, J. Phys. Chem. C 111 (2007) 19001–19008.
[39] A. Bongiorno, U. Landman, Phys. Rev. Lett. 95 (2005) 106102/1-4.
[40] L. Piccolo, D. Loffreda, F.J. Cadete Santos Aires, C. Deranlot, Y. Jugnet, P. Sautet, J.C. Bertolini, Surf. Sci. 566–568 (2004) 995–1000.
[41] F. Menegazzo, M. Manzoli, A. Chiorino, F. Boccuzzi, T. Tabakova, M. Signoretto, F. Pinna, N. Pernicone, J. Catal. 237 (2006) 431–434.
[42] H. Shi, C. Stampfl, Phys. Rev. B 76 (2007) 075327 (14).
[43] E.M. Fernández, P. Ordejón, L.C. Balbás, Chem. Phys. Lett. 408 (2005) 252–257.
[44] J.T. Miller, A.J. Kropf, Y. Zha, J.R. Regalbuto, L. Delannoy, C. Louis, E. Bus, J.A. Van Bokhoven, J. Catal. 240 (2006) 222–234.
[45] B. Hvolbæk, T.V.W. Janssens, B.S. Clausen, H. Falsig, C.H. Christensen, Jens K. Nørskov, NanoToday 2 (2007) 14.

[46] Q. Sun, P. Jena, Y.D. Kim, M. Fischer, G. Ganteför, J. Chem. Phys. 120 (2004) 6510–6515.
[47] Y.D. Kim, M. Fischer, G. Ganteför, Chem. Phys. Lett. 377 (2003) 170–176.
[48] M.S. Chen, D.W. Goodman, Catal. Today 111 (2006) 22–33.
[49] I.N. Remediakis, N. Lopez, J.K. Nørskov, Angew. Chem. Int. Ed. 44 (2005) 1824–1826.
[50] S.S. Pansare, A. Sirijaruphan, J.G. Goodwin Jr., J. Catal. 234 (2005) 151–160.
[51] E. Bus, J.T. Miller, J.A. van Bokhoven, J. Phys. Chem. B 109 (2005) 14581–14587.
[52] H. Berndt, I. Pitsch, S. Evert, K. Struve, M.-M. Pohl, J. Radnik, A. Martin, Appl. Catal. A 244 (2003) 169–179.